

Mesoscale modelling studies of microemulsions

C. A. Bearehell and D. M. Heyes*

Department of Chemistry, School of Physics and Chemistry, University of Surrey,
Guildford, UK GU2 7XH

Received 11th June 2001, Accepted 18th September 2001

First published as an Advance Article on the web

Mesoscale simulations of microemulsions have been carried out by molecular dynamics using simple single site representations of the oil and water molecules. The surfactant molecules were represented by dimers composed of the water and oil moieties. The focus of the work is on the ternary phase diagram and the extent to which a simple model can reproduce the main features. The simulations explored some of the generic factors that determine the self-assembling characteristics of these three components. Key features of real microemulsion systems were reproduced by this very simple coarse-grained model. Simulations carried out at the centre of the triangular phase diagram followed the species spontaneously self-assemble into a bicontinuous phase. The balance, even in this part of the phase diagram, could be shifted towards micelle formation with surfactant molecules of sufficiently small radius of curvature, which caused the formation of discrete water swollen reverse micelles, and an increasing number of free surfactant molecules or water-less reverse micelles. In the more dilute limit where the oil is the major phase, water-swollen inverse micelles were observed to form in the simulations. On decreasing the radius of curvature of the surfactants, an increasing number of smaller micelles were produced. There was some evidence of finite-size effects in the computer model, in that some of the systems had a tendency to form rod-like micelles (the periodic boundary conditions removed the necessity for ‘end-capping’ which occur in real systems). These became spherical micelles when larger systems with the same relative number of each component were considered. Also for the infinite radius of curvature surfactants, the swollen micelles were found to be below ‘optimum’ size as far as surfactant interfacial coverage was concerned (there were insufficient surfactant molecules in the system to cover the single water-swollen reverse micelle). The micelles were on average spherical but showed significant departures from spherical symmetry over short periods on the time scale of the density fluctuations in the system. We derive a simple analytic model for the size of the spherical micelles, based on a modification of the classical treatment, which takes into account the volume of the headgroup. This gives much improved agreement with the computed micelle size.

Introduction

Microemulsions are thermodynamically stable three phase chemical systems of oil, water and surfactant. Their interest from a scientific, and practical point of view, is that they contain ordered microstructures of various types, depending on conditions and the chemistry of the components, which are typically on the 10–100 Å scale.^{1–4} The microscopic and macroscopic characteristics of these systems have attracted much attention. We know that a variety of phases can exist that are ubiquitous in the three phase triangular phase diagram of microemulsion systems (*e.g.*, micelles, reverse micelles and a bicontinuous phase). The question we ask in this work is, what are the minimum requirements required in the description of the constituent species to produce these phases? We report the results of many-particle off-lattice computer simulations of model microemulsion systems in an attempt to answer this question, and also to establish the relative effects of the various key molecular parameters on the occurrence of these phases, in particular the shape of the surfactant molecule. Clearly this is a highly multiparametric problem, which can only partially be addressed in a pilot study of this nature.

The first generic computational study of microemulsions was performed by Wheeler and Widom who mapped out some of the essential features of a microemulsion onto a lattice model.⁵ This treatment included immiscible ‘water’ and ‘oil’ phases, and an amphiphilic component with an affinity for water at one end and oil at the other. This lattice simulation

and others that followed predicted phases with low interfacial tension broadly corresponding to those found experimentally.^{6–10} More recently, lattice models including hydrodynamic effects have been developed to investigate the non-equilibrium flow behaviour of microemulsions. The length-scale effects and domain growth dynamics were found to be in qualitative agreement with experiment.^{11,12} An off-lattice or continuum MD model developed by Telo da Gama and Gubbins shared with these coarse-grained lattice models a lack of atomistic detail, only retaining such essential features as shape and average interaction strength.¹³ Investigation of the interfacial characteristics,^{14–17} and the self-assembly of surfactants into micelles,^{18,19} using coarse-grained MD has provided the evolution and morphology of surfactant aggregates. Two dimensional MD simulations of the dynamics of phase separation in microemulsions have also been carried out.²⁰ The pseudo-atomistic level of behaviour observed in these simulations, while inaccessible to experimental techniques, has provided qualitative insight into the structure and dynamics involved.

The results of a coarse-grained molecular dynamics, MD, simulation treatment of microemulsions are presented. Compositions at several representative points on the ternary phase diagram have been investigated, along with the effect on these phases of variable surfactant shape. The complexity of the model was kept to a minimum, while preserving what were considered to be the key aspects of a microemulsion, allowing access to the dynamical processes associated with the

formation of microemulsions to be followed usefully on a computationally accessible time scale, which would otherwise be prohibitive using a more traditional atomistic force-field approach. The model chosen was simple so that the required number of particles in the system was kept to a minimum. We consider the fact that the particles followed trajectories in 'continuous space' rather than on a lattice is an important advantageous factor, enabling curvature related features to be more realistically represented.

Computational details

The forcefield was reduced to the bare essentials to describe the interaction of the component species of a microemulsion on the scale of the molecule rather than on the atomistic scale. MD simulations have been used before to investigate the interfacial behaviour and self-assembly processes at work in these systems.^{14–19} However, those simulations did not study the phase behaviour of the three component systems, but rather the surfactant behaviour at the interface of water and oil, and at low fractions of surfactant to equal proportions of oil and water. MD simulations studying the phase separation dynamics of microemulsions have been undertaken,²⁰ however, the simulations only studied the effect of different surfactant concentrations with equal amounts of oil and water. The simulations reported here are similar to those used elsewhere,^{14–19} but with the additional feature that the variations in surfactant geometry have been covered in a more comprehensive and systematic way. The relative compositions of each species were chosen carefully to focus on important domains of system where different classes of self-assembly are expected.

Simulation model

The computational model used was inspired by the work of Telo da Gama and Gubbins,¹³ and following studies.^{14–20} In the model we did not include any polarity or hydrogen bonding facility for the water molecules and head-groups. The system was described in terms of two types of particle, which we refer to as 'water' and 'oil'. The 'water' and 'oil' species mimic the real systems in being immiscible. The immiscibility of these two particle types was achieved by implementing attractive interactions between particles of the same type, while those of opposite type only interacted *via* an excluded volume repulsive force law. Model surfactants were represented by connecting a water particle to an oil particle using a harmonic spring potential, as illustrated in Fig. 1(a). The head group of the surfactant (water particle) interacted with attractive interactions with other head groups and water particles, but repulsively with oil particles. The converse was true for the tail group of the surfactant. The interparticle interactions were described by a generalised Lennard-Jones 12-6 potential,³

$$U(r_{ij}) = 4\epsilon_{ij} \left[\left(\frac{\sigma_{ij}}{r_{ij}} \right)^{12} - (2\delta_{\alpha_i\alpha_j} - 1) \left(\frac{\sigma_{ij}}{r_{ij}} \right)^6 \right] \quad (1)$$

where ϵ_{ij} is the equilibrium well depth between particles i and j , r_{ij} , the centre-to-centre separation and σ_{ij} the molecular 'diameter' between the Lennard-Jones, LJ, particles i and j . The mixing rule,

$$\sigma_{ij} = (\sigma_{\alpha_i} + \sigma_{\alpha_j})/2 \quad (2)$$

was used, where α_i is the particle class (*i.e.*, oil or water moiety) LJ diameter of the i th particle. The Kronecker delta function, $\delta_{\alpha_i\alpha_j}$,

$$\delta_{\alpha_i\alpha_j} = \begin{cases} 0 & \alpha_i \neq \alpha_j \\ 1 & \alpha_i = \alpha_j \end{cases} \quad (3)$$

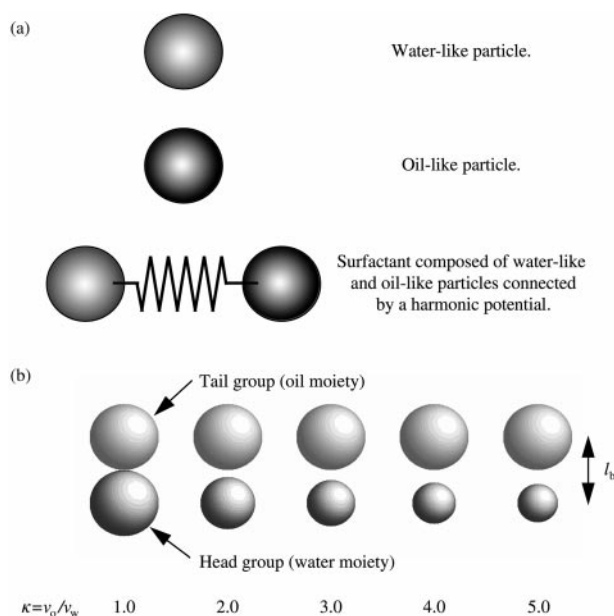


Fig. 1 Schematic representation of the species in the model microemulsion MD simulations. The surfactant bond length, l_b and oil particle to water particle ratio volume $\kappa = v_o/v_w$, are shown in the diagram.

indicates that in eqn. (1), particles of the same type interacted with a dominant attractive component at long range, while those of opposite types interacted repulsively (of course all species combinations are repulsive at separations less than $\sim \sigma_{ij}$ see eqn. (1)). A harmonic potential was used to describe the bond between the head and tail (water-like and oil-like respectively) of the surfactant particle,

$$U_{\text{stretch}} = \frac{k_s}{2} (r_{ij} - l_b)^2 \quad (4)$$

where k_s is the spring constant, l_b is the equilibrium bond length, which was given the value of the diameter of the oil particle, σ_{oil} . The separation between the water and oil particles within the surfactant molecule is r_{ij} . The spring constant was set so that during the simulation 90% of the connected units were within 2% of the equilibrium bond length.

The system parameters and properties are quoted in terms of the LJ parameters for the oil particles (energy, length, mass: ϵ, σ, m). The dimensionless quantities and units (in brackets) are: number density ($\rho\sigma^3$), temperature ($k_B T/\epsilon$), energy (E/ϵ), pressure ($P\sigma^3/\epsilon$), time ($(\epsilon/m\sigma^2)^{1/2}t$) and force ($f\sigma/\epsilon$). The simulations were carried out at an average reduced density of $\rho\sigma^3 = \rho^* = 0.8$ and reduced temperature, $T^* = 0.8$. The reduced force constant for the surfactant intramolecular potential was, $k_s^* = 10^4$ and the time step, $\Delta t^* = 0.005$.

System composition

Each simulation was started with N_w water and N_o oil molecules distributed randomly on a face centred cubic (fcc) lattice. A number of surfactant molecules, N_s , were constructed by connecting pairs of adjacent water and oil molecules, again without any spatial preference. Each system consisted of 2916 separate LJ sites. The ratio of each component was chosen to study a specific point of the ternary phase diagram, which is usually represented as a triangular diagram.²¹ Two regions of this phase diagram were investigated, one point at the centre (with the ratio $N_o : N_w : N_s$ equal to 1 : 1 : 1) and three points in the oil rich portion of the phase diagram with $N_o : N_w : N_s$ equal to 20 : 1 : 1, 20 : 2 : 1 and 20 : 1 : 2. Henceforth, simulations

Table 1 The number of each component for simulations performed at four points on the ternary phase diagram. N_o , N_w and N_s are the number of oil, water and surfactant molecules in the simulation cell, respectively

Simulation type	Symbol	$N_o : N_w : N_s$	N_o	N_w	N_s	% surfactant
'Concentrated'	C	1 : 1 : 1	729	729	729	33.33
'Dilute'	Da	20 : 1 : 1	2532	128	128	4.60
'Dilute'	Db	20 : 2 : 1	2404	256	128	4.60
'Dilute'	Dc	20 : 1 : 2	2276	128	256	9.62

carried out at the centre of the phase diagram will be referred to as 'concentrated', and given the symbol C. Those in the oil-rich part of the phase diagram are referred to as 'dilute', and given the main symbol D. Table 1 shows the number of each of the components at the phase points simulated. Starting configurations were those in which the species were randomly placed in the cubic simulation cell.

Variation in surfactant geometry

The relative composition of water, oil and surfactant and also the geometry of the surfactant species affect the self-assembly characteristics of microemulsions. To study the effect of changing surfactant shape on the phase behaviour, it would have been possible to have combined several water and oil molecules to achieve a desired geometry (see ref. 15 for example). This would have had the disadvantage, though, that the linking together of many LJ sites would have decreased the number of separate molecules in the system, effectively reducing the system size. This problem would have been particularly acute for concentrated simulations where a great number of surfactant molecules are required. This could have been resolved by simply increasing the number of LJ sites in the simulation, to accommodate a greater number of the extended surfactant particles. However, this could have only been achieved at some considerable computational cost. The alternative, 'geminal' surfactant construction adopted, with surfactant shape altered by changing the relative diameters of the water and oil moieties, had many advantages in this respect. This strategy is illustrated in Fig. 1(b). The parameter that defines the shape of the surfactant, κ , is the ratio of the volume of the oil particle to the volume of the water particle, v_o/v_w . Being the normal majority phase, the oil particles were used as the reference, and therefore the water species will be seen in this figure to diminish in size with increasing κ . This could equivalently be viewed as a relative increase in the size of the surfactant tail and oil molecule compared with the head group (*i.e.*, with increasing chain length).

To change the geometry in a systematic and quantifiable way, simulations run at each phase point were repeated a further four times, each with a decrease in the volume of the

Table 2 Nomenclature for the concentrated class of systems with variable surfactant shape, showing the variation in the diameter of water and oil particles for simulations at each phase point. The oil-to-water molecule volume ratio, $\kappa = v_o/v_w$ and water particle diameter, σ_w , in terms of the oil particle diameter are shown for the 'concentrated' simulations C1–C5

Simulation	κ	σ_w
C1	1	1.000
C2	2	0.794
C3	3	0.693
C4	4	0.630
C5	5	0.585

water particle ($\pi\sigma_w^3/6$). This resulted in five simulations with water particle to oil particle volumes, κ , of 1.0, 2.0, 3.0, 4.0 and 5.0. Note that the radius of curvature of the surfactant molecules decreases along this series. The radius of curvature is infinite for $\kappa = 1$. Table 2 gives the details of the water species for the five C-class simulations performed.

Simulation technical details

Five simulations were performed at each phase point. Each simulation consisted of 2×10^5 time steps using the Verlet leapfrog algorithm to integrate the equations of motion, with temperature control achieved by velocity scaling. Simulations were carried out at constant volume. All the molecular dynamics simulations reported here were made with home-produced software written in FORTRAN 90 and implemented on a SG Power Challenge at the University of Surrey Computer Centre.

First we will consider the concentrated ('C') systems, which occur in the middle of the phase diagram given in Table 1.

Concentrated systems

An initial random distribution of oil, water and surfactant was allowed to evolve over a period of 1000 reduced time units. In Fig. 2 we show the final configuration for the extreme cases (a) $\kappa = 1$ and (b) $\kappa = 5$. In these figures, the oil particles have been omitted from the figure to help clarify the structures formed by the remaining components. The 'oil' parts of the surfactant molecules are shown, however. At a late time, $t = 1000$, phase separation of water and oil was complete and surfactant particles are seen to be localised between the oil and water phases. In the $\kappa = 1.0$ case (equal sized heads and tails in the surfac-

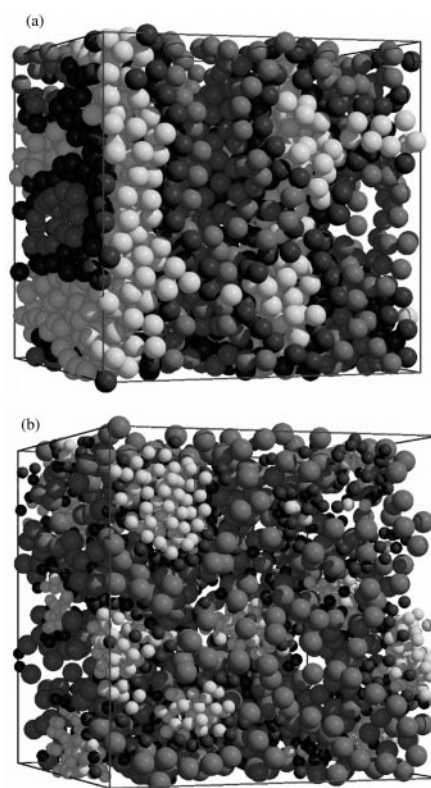


Fig. 2 Snapshots of the concentrated simulations, (a) C1 for $\kappa = 1.0$, and (b) C5 for $\kappa = 5.0$. Water particles are shown as white spheres, surfactant headgroups as black spheres and surfactant tails as dark grey spheres. The oil particles are omitted for clarity.

tant) the particles self-assembled into ‘sheets’ of water and surfactant connected by channels of water, which look like the usual picture of the bicontinuous phase found in microemulsion systems at this location in the ternary phase diagram. For $\kappa > 1.0$, we found, however, that this bicontinuous structure does not form. Fig. 2(b) shows an instantaneous configuration taken from a concentrated simulation in which the oil particles (and tail groups) were five times larger than water particles and head groups ($\kappa = 5.0$). Instead of a bicontinuous phase, the water particles are concentrated into micellar-like pockets distributed through the simulation cell. The bicontinuous phase has been disrupted and only the oil phase (not shown explicitly in the figure) is continuous. This different behaviour may be attributed to the decreased radius of curvature, R_s , of the surfactant, which promotes an increasingly curved interface between water and oil, and as a contributory factor, a decrease in the relative volume fraction of the water compared with oil molecules. This made it less probable that the system would have exhibited a continuous water phase. The snapshots of the particle assemblies also show an increase in the number of surfactant particles that are not associated with any water molecules. Since the water particles were organised into roughly spherical aggregates, the area of water exposed to the oil particles was reduced, and the total surface area the surfactants were able to cover was greater than the exposed surface area of water. This drove the excess surfactants into the bulk oil phase, resulting in an increase in the number of free surfactants. Such re-equilibration behaviour may have been responsible for the slow late-time dynamics observed in high surfactant concentration simulations elsewhere.²⁰ Consequently, a greater excess of surfactants was observed progressively through simulations C1–C5.

Pair distribution functions

The pair distribution functions between various species provide a more quantitative characterisation of the phase changes. The pair distribution functions, $g_{ww}(r)$ and $g_{oo}(r)$ are the pair distribution function between the water-like and oil-like species, respectively. Fig. 3 shows the radial distribution function for water particles (including surfactant head groups) computed from simulations C1–C5. Results are plotted against particle centre-to-centre separation, in units of the water particle radius. All examples show peaks associated with the first and second coordination shells, which are typical of the liquid state, and clearly reflecting the phase separation of the water

into pockets in these systems. The heights of the first coordination shell peaks show a pronounced increase as the water particle size decreases. This reflects the progressive partitioning of the water molecules, and the relative increase in the volume of the oil component compared to the ‘water’. As the water molecules decreased in size, and κ increased the local water number density in the micelle-like regions was increased when compared to the average number density across the whole system. This in turn caused $g(r)$ to increase in height at low separation values with increasing κ . In addition, longer-ranged correlations appeared in the inter-micelle distance range as a minimum in the pair distribution function. Simulations C2–C5 show a featureless minimum in the pair distribution function between four and six oil diameters, presumably because of the depletion of water particles in the oil phase in this region as they aggregate into micelles. The value of the separation at which this minimum occurs should correspond to half the average separation between the centre of mass of the micelles. These separations are 5.4, 4.9, 4.6 and 4.4 σ_{oil} for simulations C2–C5, respectively. The decrease in these values with decreasing water particle size is a result of the fact that many more and smaller micelles were formed with increasing κ , which reduced the average mean separation between the micellar clusters. The radial distribution function for simulation C1 in this range is very different to those from simulations C2–C5. This reflects the difference in long-range structure between the bicontinuous structure observed in simulation $\kappa = 1$ compared to the discrete micelles formed in all of the other simulations at this phase point. Nevertheless a minimum still appears in $g_{ww}(r)$ on this simulation at about 5.0 oil diameters, with the pair distribution function oscillating with a period of about one oil diameter even in the intermediate range (thus reflecting both short range and long-range structural features). This would suggest that the centres of the ‘layers’ of water-like particles are separated from the centres of the oil-like ‘layers’ by about five oil particle diameters. There is a monotonically decaying relationship between the inter-micellar separation and the volume ratio, κ , as more micelles are created with decreasing κ .

Cluster analysis

Since the simulations resulted in aggregated structures of water and surfactant, a useful analysis tool was to define the system in terms of component clusters of particles. The cluster was defined in terms of a local connectivity criterion, achieved by taking a sample particle, say the i th particle, and calculating the separation between this particle and others in the same simulation cell. Let another particle be the j th particle. If particle j passes the criterion,

$$r_{ij} \leq r_{cl} \quad (5)$$

where r_{cl} is a critical separation value and r_{ij} is the separation between the two, then particle j is deemed to be in the same cluster. Any particles that are not in this cluster are used as ‘starter’ particles for new clusters. The cluster statistics can be quite sensitive to the choice of the critical separation value, r_{cl} , although values in the range 1.3–1.9 σ_{oil} were mainly explored as they have the most physical significance. We found that a value of $r_{cl} = 1.6$ gives a description of the cluster consistent with what is seen in the pictures of the instantaneous configurations. The number of isolated water-like particles increases through simulations C1 to C5. Table 3 shows that the number of free surfactant molecules increases as κ decreases. The maximum number of particles in a single cluster decreases through simulation series C1 to C5. The average number of particles in the clusters goes from containing all water molecules in simulation C1 ($\kappa = 1.0$), reflecting the continuous water structure, to values ($\kappa > 1.0$) representative of the

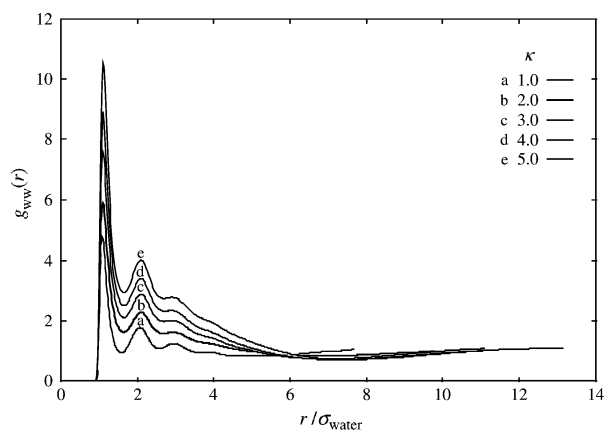


Fig. 3 Average pair distribution function for water–water interactions. ‘Free’ and surfactant water contributions are included. Results for all κ (increasing from bottom to top) values are presented on the figure.

Table 3 Results of a cluster analysis performed on the surfactant headgroup particles taken from the final configuration of simulations C1–C5. Simulations C1 to C5 are distinguished by the oil particle volume-to-water particle volume ratio, κ . The critical separation value, r_{cl} , is expressed in units of σ_{oil} . The number of isolated particles, $N_{isolated}$, the maximum number of particles in a cluster, N_{max} , the number of clusters and the average number of particles in a cluster, $\langle N_{cluster} \rangle$, are shown. We have $r_{cl}/\sigma_{oil} = 1.6$ here

κ	$N_{isolated}$	N_{max}	Number of clusters	$\langle N_{cluster} \rangle$
1	0	729	1	729
2	15	307	10	57
3	60	79	25	13
4	119	57	15	7
5	167	26	13	5

number of water swollen reverse micelles. The number of isolated surfactant molecules increases dramatically with decreasing water particle volume. The maximum number of surfactants in a single cluster (called the aggregation number) decreases from simulations C1 to C5, from $N_{max} = N_s$ to $N_{max} = 26$. The average number of surfactants in a cluster drops dramatically with decreasing water particle size, again due to a greater number of reverse micelles containing no water molecules in the system.

Dilute systems

Now we turn to the oil-rich corner of the ternary phase diagram. These will be designated ‘dilute’ systems. To aid the discussion of the results, the simulations carried out in this part of the phase diagram will be referred to using the nomenclature given in Table 4.

System configurations

First we consider the Da or $N_o : N_w : N_s$ equal to 20 : 1 : 1 systems. Simulation Da1 resulted in the formation of a single water swollen micelle. The aggregate appears spherical, with surfactant molecules evenly but sparsely distributed around the water core. Simulation Da3 resulted in the creation of two water-swollen micelles (see Table 5), as the radius of curvature of the surfactant and consequently, the interface, was increased. The greater curvature of the interface promoted the formation of smaller water swollen micelles. This process was continued in simulation Da5, with five micelles being formed. All simulations showed the spontaneous self-assembly of water and surfactant molecules into water swollen reverse micelles, which is consistent with the position of the simulation composition on the ternary phase diagram.

Now we consider the Db or $N_o : N_w : N_s$ equal to 20 : 2 : 1 systems. Fig. 4 shows the final configuration for simulations

Table 4 Naming scheme for the ‘dilute’ class of simulations in which the oil species makes up the majority phase

κ	Component ratio $N_o : N_w : N_s$		
	20 : 1 : 1	20 : 2 : 1	20 : 1 : 2
1	Da1	Db1	Dc1
2	Da2	Db2	Dc2
3	Da3	Db3	Dc3
4	Da4	Db4	Dc4
5	Da5	Db5	Dc5

Table 5 Results of the cluster analysis applied to water and surfactant headgroup molecules for the dilute simulation series. The simulation index corresponds to the compositions for simulations given in Table 4. The critical separation value, $r_{cl} = 1.6 \sigma_{oil}$. The number of isolated particles, $N_{isolated}$, the maximum number of particles in a cluster, N_{max} , the number of clusters and the average number of particles in a cluster, $\langle N_{cluster} \rangle$, are given

Simulation index	κ	$N_{isolated}$	N_{max}	Number of clusters	$\langle N_{cluster} \rangle$
Da1	1	0	256	1	256
Da2	2	0	177	2	128
Da3	3	0	209	2	128
Da4	4	2	142	4	43
Da5	5	1	131	5	27
Db1	1	0	384	1	384
Db2	2	0	384	1	384
Db3	3	0	384	1	384
Db4	4	3	354	2	76
Db5	5	12	347	2	17
Dc1	1	0	384	1	384
Dc2	2	0	227	2	192
Dc3	3	2	104	5	55
Dc4	4	4	79	12	22
Dc5	5	14	88	13	12

Db1, Db3 and Db5. Oil particles have been omitted from the figure to clarify the self-assembled structures. In this series of simulations, the number of water molecules was doubled over the Da series, and the number of surfactant molecules was maintained the same. Simulation Db1 shows a single water-swollen reverse micelle. The micelle is larger than that seen in simulation Da1 and the surfactant molecules are much more sparsely distributed, as they are attempting to cover a greater surface area of water. Their stabilisation ability is therefore less. The figure from simulation Db3 also shows a single micelle, however the surfactants are more densely packed at the interface. This is presumably due to the decreased volume of the water moieties, which presented a smaller surface area to the surfactants, which could then pack more closely and effectively. Simulation Db5 resulted in the formation of multiple micelles, and a proportion of free surfactant molecules in the oil phase. This is a continuation of the trend observed for simulation Db3. Importantly, the decrease in the surface area of the water phase was greater than the decrease in area of interface the surfactant is able to cover (see later). This resulted in an excess of surfactant that could be released into the bulk oil.

We now consider the Dc series, with $N_o : N_w : N_s$ equal to 20 : 1 : 2. Fig. 5 shows the final configuration adopted by simulations Dc1, Dc3 and Dc5. This series of simulations had twice the number of surfactant molecules and the same number of water molecules as in simulation series Da. Simulation Dc1 shows the formation of a continuous ‘tube’-like structure of water surrounded by surfactant molecules running across the periodic boundaries of the simulation. This rod-shaped micelle may have been promoted by the periodic boundary conditions. The periodic boundary conditions obviated the necessity for ‘end capping’, which would be present in real systems. System Dc3 results in a break up of the ‘tubular’ structure seen in simulation Dc1, into a mixture of water-swollen reverse micelles and reverse micelles comprising only surfactants. This may again have been due to an ‘excess’ of surfactant molecules than was required to cover the water particles at the oil–water interface. The formation of the micellar species is due to the increasingly favoured curved interface brought about by the decrease in the radius of curvature of the surfactant. This process continued for system Dc5, with more numerous but smaller water swollen reverse micelles being formed.

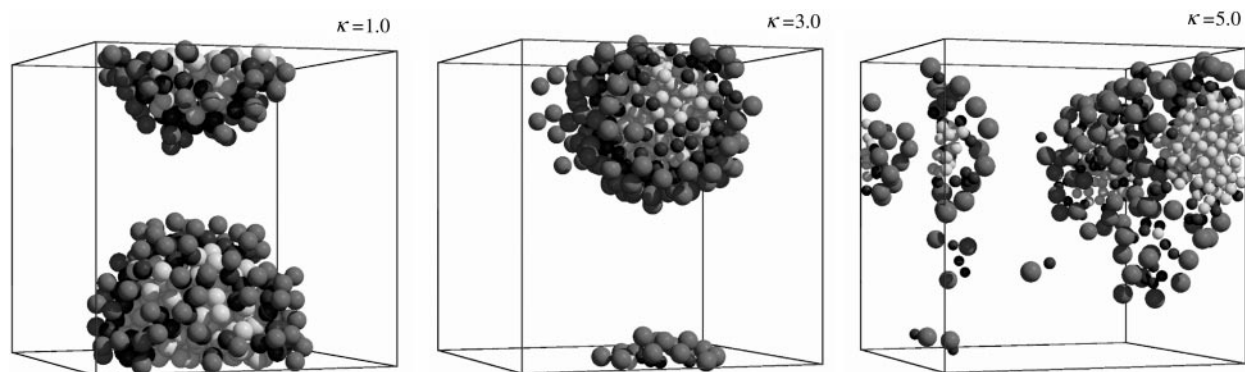


Fig. 4 Final system configurations adopted by the species in simulations Db1, Db3 and Db5. White spheres depict the water particles, surfactant headgroups by black spheres and surfactant tails by dark grey spheres. Oil particles have been omitted from the snapshots to clarify the self-assembled structures. The oil phase is in the majority, and there are twice as many water molecules as surfactant molecules. The periodic boundary conditions have the effect of appearing to break up the model micelle formed.

Cluster analysis for the dilute systems

In this section an analysis of the clusters is presented for the dilute systems. Table 5 shows the results of the cluster analysis when applied to the water and surfactant headgroup moieties in all simulations performed in the oil rich portion of the microemulsion ternary phase diagram. For simulation series Da (with a ratio of oil to water to surfactant of 20 : 1 : 1) very few isolated water-like particles are observed in the final system configuration. The maximum number of particles in a cluster generally decreased with increasing κ , but with an inconsistently high value for simulation Da3. The number of clusters identified by the analysis increased from simulation Da1 to Da5, again with an inconsistent value observed for simulation Da3. This may be indicative of the merging or splitting of two micelles at the point in the simulation at which the analysis was performed. In this case there would appear to be two clusters, when there are actually three, and the maximum number of particles in a cluster would also be larger than expected. The average number of particles in the clusters identified at the end of the simulations decreased as the value of κ increases, with simulation Da3 showing an anomalously high value.

These observations are consistent with expectations based on a decreasing radius of curvature, R_s , through Da1–Da5, which promotes the formation of an increasingly curved interface between oil and water. To accommodate a larger curvature with optimum packing, the reverse micelles must become smaller. Consequently, the number of water molecules the micelles can contain also decreased as κ increases. The larger micelles broke up into a greater number of smaller

micelles. The volume of water that individual micelles were able to hold decreased more rapidly than the total volume of water in the system, as κ moved to higher values.

The cluster statistics of simulation series Db (with an oil : water : surfactant number ratio of 20 : 2 : 1) is different to that of simulation series Da (20 : 1 : 1), as revealed in Table 5. Simulations Db1 to Db3 show no change in the number of isolated particles, the maximum and average number of particles *per* cluster and the number of clusters, as κ increases. All three simulations produce only one micelle presumably because the larger number of water molecules in the micelle of the Db series stabilises a single micelle against moderate changes in the shape of the surfactant molecule. As κ increases to 4.0 and 5.0 the results of the cluster analysis are quite different. Isolated particles (presumably surfactant molecules) had appeared, indicating the water interface had become saturated. Multiple clusters are observed, although for both simulation Db4 and Db5, the number of particles in the two clusters formed during each simulation was very different, perhaps indicative of a single micelle with the optimum size and a further micelle composed of the ‘spare’ water and surfactant molecules.

The results of the cluster analysis for all water-like particles in series Dc (with an oil to water to surfactant ratio of 20 : 1 : 2) are also shown in Table 5. The number of isolated particles and the number of clusters in the simulation increased with κ , while the maximum and average number of particles in each cluster decreased. Simulation Dc1 resulted in a continuous ‘tube’ like structure, while Dc2 exhibited interconnected pockets of water covered by surfactants. For simulations Dc3 to Dc5 an increasing number of discrete water-swollen micelles

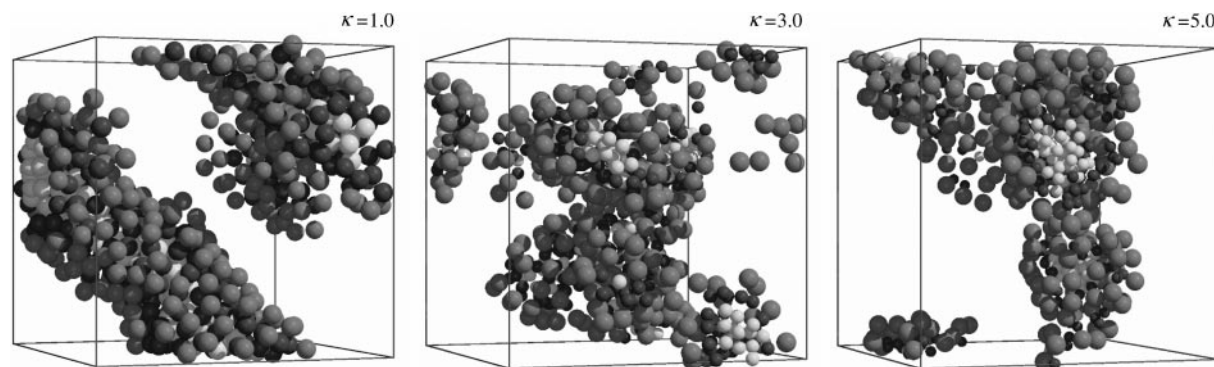


Fig. 5 Snapshots of the final configurations adopted by simulations Dc1, Dc3 and Dc5, where there are twice as many surfactant molecules as water molecules as for the system in Fig. 4; otherwise as for Fig. 4.

of progressively decreasing size were observed. There were generally a greater number of isolated surfactants than isolated water molecules, which is not surprising as there were relatively more of them in this simulation, and the surfactant molecules only had to occupy a layer at the interface between the water and oil particles. More surfactants were found in the bulk oil phase once the interface has been saturated. This would explain why simulations where the interface was sparsely populated by surfactants (those with a single micelle, Da1, Db1, Db2 and Db3) were found to have very few isolated surfactant molecules in the bulk oil.

Micelle size and shape

An analysis of the micelle shape and surface contours was made at each timestep and these functions were averaged over time. A cluster analysis was performed to identify each micelle present. The centre of mass was calculated for each micelle, and the spherical coordinates of each surfactant relative to the centre of mass were found. A B-spline interpolation routine was then employed for each micelle to find the radial component of the spherical coordinates, for surfactant heads and tails, at equal intervals of the angular components. An average size and shape for the micelles present at that timestep were then calculated by averaging the value of the radial coordinates at the angular coordinates chosen for each micelle. This process was repeated at each timestep and an overall average of the position of the surfactant heads and tails obtained at regular angular intervals of time.

Fig. 6 shows a graphical representation of the single cluster Da1 as an accumulated time average from an arbitrary starting point. The average size and shape is represented by two 'cages', an outer cage corresponding to the surfactant tails and an inner cage showing the surfactant headgroups. The cluster size and shape analysis was performed and

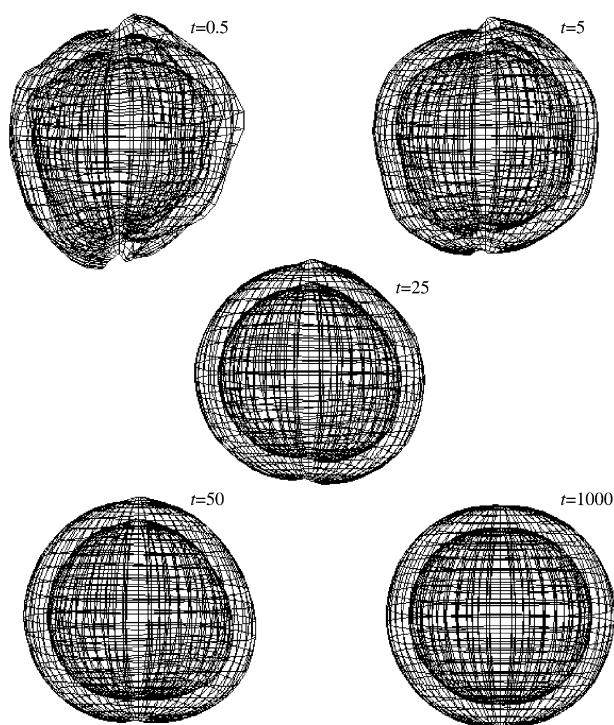


Fig. 6 A contour grid representation of the average surfaces of the micelles present in simulation Da1. The outer grid traces out the position of the surfactant tails and the inner grid shows the position of the surfactant headgroups. Micellar shapes are averaged over time intervals up to $t=0.5, 5, 10, 25$ and 50 .

averaged over intervals up to $t=0.5, 5, 25, 50$ and 1000 . At $t=0.5$, the micelle had a very uneven surface. At $t=5$, the surface of the micelle was smoother, with little indication of individual surfactants. However, the overall shape was irregular and not particularly spherical. At times of $t=25$ and $t=50$ the surface of the micelle had now become more uniform as the positions of individual surfactants were averaged. There are still noticeable differences from a sphere though. At $t=1000$, the averaged shape of the micelle was very close to being spherical, with a smooth and symmetrical surface topography, demonstrating that the shape fluctuations cancel out over a long period but are still accessible within the duration of typical simulation.

A quantitative means of measuring the shape of the micelle was also used, employing the asphericity order parameter, A_3 , of Rudnick and Gaspari,²²

$$A_3 = \frac{\langle \sum_{i \neq j} (\lambda_i - \lambda_j)^2 \rangle}{2 \langle (\sum_{i=1}^3 \lambda_i)^2 \rangle} \quad (6)$$

where $\langle \dots \rangle$ denotes an ensemble average and l_i are the three principle moments of inertia of the surfactant tailgroups in the micelle. The principle moments of inertia are obtained by diagonalisation of the 3×3 inertia tensor, T , in which the elements are,

$$T_{\alpha\beta} = \frac{\sum_{i=1}^{N_s} m_i (r_i^\alpha - r_{\text{com}}^\alpha)(r_i^\beta - r_{\text{com}}^\beta)}{\sum_{i=1}^{N_s} m_i} \quad (7)$$

where N_s is the number of surfactant tail particles in the micelle, α and β are x, y or z , and m_i is the mass of the i th tail particle ($m_i = 1.0$). The α component of the position vector of particle i is r_i^α , and r_{com}^α is the α component of the centre of mass of the micelle. We have, $A_3 = 0$ for a perfect sphere, $1/4$ for a uniform, infinitely thin, circular disk and 1.0 for an infinitely thin rod. Fig. 7 follows the instantaneous value of A_3 for simulation Da1 over a time interval of $t=1000$. The micelle was generally spherical as the asphericity order parameter fluctuated around a low value of ~ 0.015 and did not rise above a value of ~ 0.075 at any time. Short-lived ellipsoidal distortions in the shape of the micelle occurred over relatively short time intervals, which show up as peaks in the plot of A_3 against time. The accumulated average shape was calculated from the time averaged inertia tensor, $\langle T_{\alpha\beta} \rangle$, which was used to calculate the 'average' principle moments of inertia. An accumulated average was,

$$A_3^{\langle T_{\alpha\beta}(t) \rangle}(t) = \frac{\langle \sum_{i \neq j} (\langle \lambda_i(t) \rangle - \langle \lambda_j(t) \rangle)^2 \rangle}{2 \langle (\sum_{i=1}^3 \langle \lambda_i(t) \rangle)^2 \rangle} \quad (8)$$

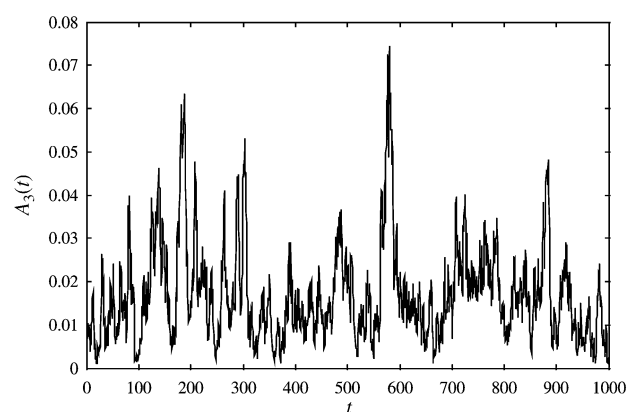


Fig. 7 Time dependant behaviour of the instantaneous asphericity order parameter, A_3 , for the single micelle observed in the dilute simulation Da1 from eqn. (6).

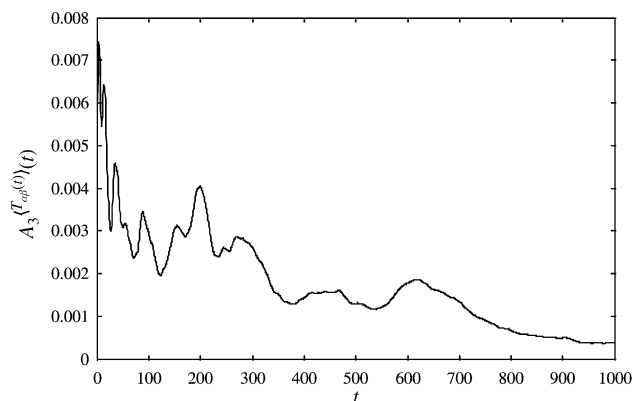


Fig. 8 Time dependant behaviour of the asphericity order parameter, $A_3^{(T_{\alpha\beta})}(t)$, from eqn. (8), calculated from the accumulated average of the inertia tensor, for the single micelle observed in the dilute simulation Da1.

where $\langle \lambda_i(t) \rangle$ is the average of the principle moments of inertia over time t , calculated by diagonalisation of the inertia tensor, $\langle T_{\alpha\beta}(t) \rangle$, averaged over time t . Fig. 8 shows the accumulated average asphericity order parameter, as calculated from eqn. (8), against time. The plot shows that the order parameter starts at the same value as the instantaneously calculated value, A_3 , and then decreases to reach a value of ~ 0.0005 . This is consistent with an average spherical micellar shape, shown in Fig. 6. The average value of the instantaneous asphericity order parameter (as shown in Fig. 6) is 0.02 ± 0.01 . Since the value calculated from the time averaged inertia tensor is so much lower, shape fluctuations in the micelle are seen to be quite appreciable, but relatively short-lived.

Comparison of cluster size with theory

It has been shown for microemulsions in the micellar regime that the average radius of the micelles, R , that self-assemble in the system is determined by the ratio of the concentration of surfactant, [surfactant] to dispersed phase, $[H_2O]$, the projected area of the head-group of the surfactant on the inside of the micelle, a_{surf} , and the volume of the dispersed phase molecules, v_{disp} .^{3,23} It has been found to a good approximation that,²⁴

$$R = \frac{3v_{\text{disp}}}{a_{\text{surf}}} \frac{[H_2O]}{[\text{surfactant}]} \quad (9)$$

where R defines the radius of the micellar core shown in Fig. 9(a). The derivation of this formula is as follows. The volume of the core, V_{core} , is given by,

$$V_{\text{core}} = N_{\text{disp}} v_{\text{disp}} = 4\pi R^3/3 \quad (10)$$

where N_{disp} is the number of dispersed phase molecules in the core. The surface area of the core is given by,

$$A_{\text{core}} = N_{\text{surf}} a_{\text{surf}} = 4\pi R^2 \quad (11)$$

Combining eqns. (10) and (11) gives,

$$\frac{V_{\text{core}}}{A_{\text{core}}} = \frac{N_{\text{disp}} v_{\text{disp}}}{N_{\text{surf}} a_{\text{surf}}} = \frac{R}{3} \quad (12)$$

which upon rearrangement gives,

$$R = \frac{3v_{\text{disp}}}{a_{\text{surf}}} \frac{N_{\text{disp}}}{N_{\text{surf}}} = \frac{3v_{\text{disp}}}{a_{\text{surf}}} \frac{[H_2O]}{[\text{surfactant}]} \quad (13)$$

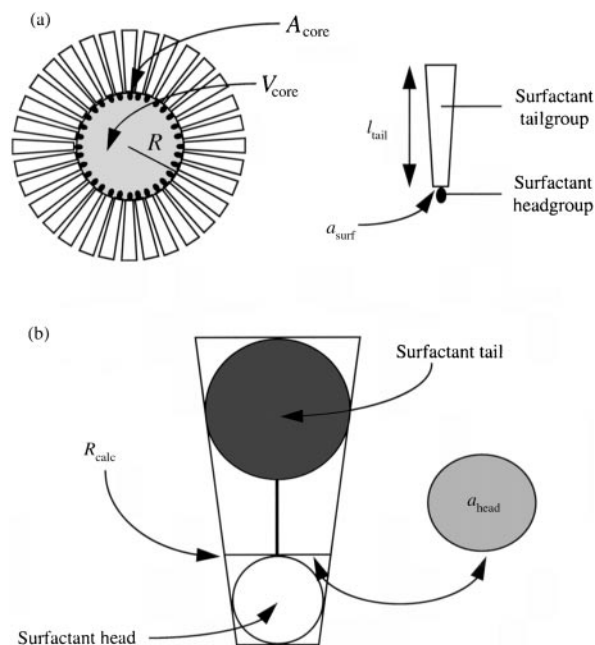


Fig. 9 (a) Schematic diagram of the model used to derive eqn. (13). The radius of the micellar core is R , the volume of the core V_{core} , the surface area of the micellar core A_{core} , the area covered by the surfactant A_{surf} and the length of the surfactant tail l_{surf} . (b) Schematic diagram showing the circular area behind the headgroup of the surfactant, a_{head} , projected onto the surface of the micellar core.

where water is the dispersed phase, and the water and surfactant molecules are assumed to exist only in micelles of the same size. The first form of eqn. (13) allows us to test the simulation against this theory since the number of water and surfactant molecules are known and the volume of the dispersed water phase and the area of the surfactant molecules can be calculated. The effective volume per water molecule occupied by the dispersed water particles is approximately,

$$v_{\text{disp}} = \frac{v_{\text{water}}}{\eta_{\text{RCP}}} \quad (14)$$

where $\eta_{\text{RCP}} = 0.637$ is the volume fraction for dense random packing of hard spheres,²⁵ and v_{water} is the volume of the water molecules,

$$v_{\text{water}} = \pi \sigma_{\text{water}}^3/6 \quad (15)$$

Similarly, the effective area covered by a single surfactant is,

$$a_{\text{surf}} = \frac{a_{\text{head}}}{\zeta_{\text{RCP}}} \quad (16)$$

where $\zeta_{\text{RCP}} = 0.820$ is the area fraction for random close packing of hard discs,²⁶ (two dimensions) and a_{head} is the area of the surfactant behind the head group (see Fig. 9(b)).

Table 6 presents the values of the constants required to calculate a theoretical micelle size from eqn. (13). Fig. 10(a) shows a comparison of the calculated average micellar radius from the simulation, R_{obs} , and the theoretical average micellar radius, R_{calc} , from eqn. (13). The observed micellar radius, R_{obs} , was taken from the average surfactant tail positions calculated in the previous section, minus the distance between the centre of the tailgroup particle and the 'back' of the headgroup,

$$R_{\text{obs}} = R_{\text{tail}} - l_b + \sigma_w/2 \quad (17)$$

where R_{tail} is the average radial distance of the surfactant tail particle from the centre of mass of the micelle, l_b is the surfactant bond length and σ_w is the diameter of the water-like moiety of the surfactant. As can be seen from Fig. 10(a), the agreement

Table 6 Values of the constants required to calculate the theoretical average micellar radius, R_{calc} , from eqn. (13). The radius of the oil and water molecules are, r_{oil} and r_{water} respectively, the volume of these particles are v_{oil} and v_{water} . The circular area of the surfactant projected onto the micellar core and the surfactant tail length are a_{head} and l_{tail} which are defined in Fig. 9

κ	r_{oil}	v_{oil}	r_{water}	v_{water}	a_{head}	l_{tail}
1	0.5	0.524	0.500	0.524	0.785	0.500
2	0.5	0.524	0.397	0.262	0.602	0.603
3	0.5	0.524	0.347	0.174	0.503	0.653
4	0.5	0.524	0.315	0.130	0.438	0.685
5	0.5	0.524	0.293	0.104	0.393	0.707

between theory and the observed values is quite poor for all simulations. The simulation value is larger than the prediction of eqn. (13) by as much as a factor of two. The model proposed for the theoretical size is clearly inadequate to represent these model micelles. One of the assumptions made in constructing this model is that the surfactant headgroup has zero volume and therefore does not affect the volume of the water swollen micellar core. This assumption is perhaps justified when dealing with a system of real surfactants with very small head groups, especially if the water core is large. The headgroups of the surfactants in these simulations are comparatively that much larger, and the volume of the water-like part should be taken into account in any theoretical model. The volume of the core, V_{core} , therefore must include the contributions from headgroups. Eqn. (10) needs to be revised as follows,

$$V_{\text{core}} = N_{\text{disp}} v_{\text{disp}} + N_{\text{surf}} v_{\text{surf}} = \frac{4\pi R^3}{3} \quad (18)$$

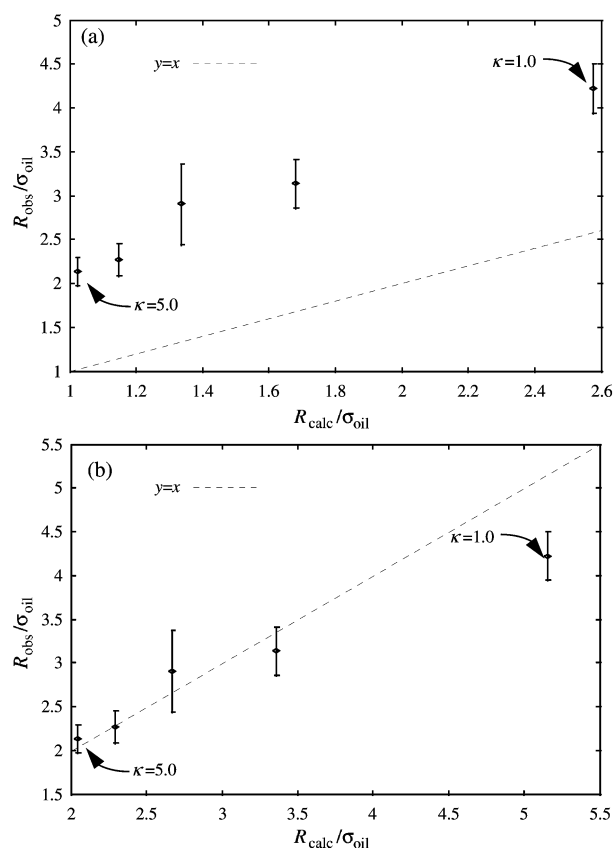


Fig. 10 (a) Comparison of the computed and calculated values for the average micellar radius for simulation series Da, here R_{calc} is defined in eqn. (13) and R_{obs} is defined in eqn. (17). (b) Comparison of observed and calculated values for the average micellar radius for simulation series Da using the alternative model of eqn. (19).

Since in this model, $v_{\text{disp}} = v_{\text{surf}}$ we can make the further simplification to a form analogous to eqn. (13),

$$R_{\text{calc}} = \frac{3v_{\text{disp}}(N_{\text{disp}} + N_{\text{surf}})}{a_{\text{surf}} N_{\text{surf}}} \quad (19)$$

Eqns. (14) and (16) still apply in this revised model.

Fig. 10(b) shows the results of the comparison between the calculated and observed average micellar radii using the alternative treatment of eqn. (19). The data clearly shows a much-improved agreement with the simulation data. Data from the simulations Da2 to Da5 are, within statistics, in excellent agreement with the theoretical line, while only the radii of the micelles in simulation Da1 are visibly lower than the predicted value. This may be due to the fact that the simulation does not contain enough water to form a single micelle of the optimum size. Application of this model may only be relevant to simulations with more than one micelle, thus ensuring that at least one of the micelles present has achieved an 'optimum' or thermodynamically most stable size. The number of water molecules is insufficient to accommodate an optimum representation of the micellar species for the low κ values. Simulations Db and Dc show the same trends. Fig. 11 shows a plot of the observed micellar radius against the calculated radius for all simulations that self-assembled into discrete water-swollen reverse micelles. There is now a good agreement between the observed and calculated micellar radii for simulation series Da to Dc, for the smaller micelles at least.

The total surface area presented to the interface by water by a single micelle can be expressed as follows,

$$\begin{aligned} A_{\text{water}} &= 4\pi R_{\text{water-core}}^2 \\ &= 4\pi \left(\frac{3\pi N_{\text{water}} v_{\text{disp}}}{4} \right)^{2/3} \\ &= 4\pi N_{\text{water}}^{2/3} \left(\frac{3\pi v_{\text{disp}}}{4} \right)^{2/3} \end{aligned} \quad (20)$$

where,

$$R_{\text{water-core}} = \left(\frac{3\pi N_{\text{water}} v_{\text{disp}}}{4} \right)^{1/3} \quad (21)$$

Hence the surface area presented to the interface by a single spherical micelle varies as the power of 2/3 of the number of water molecules. The total surface area that the surfactant molecules are able to cover, however, varies according to N_{surf} ,

$$A_{\text{surf}} = N_{\text{surf}} a_{\text{surf}} \quad (22)$$

Consequently increasing the number of particles in the simulation, while preserving the ratio of the number of water to

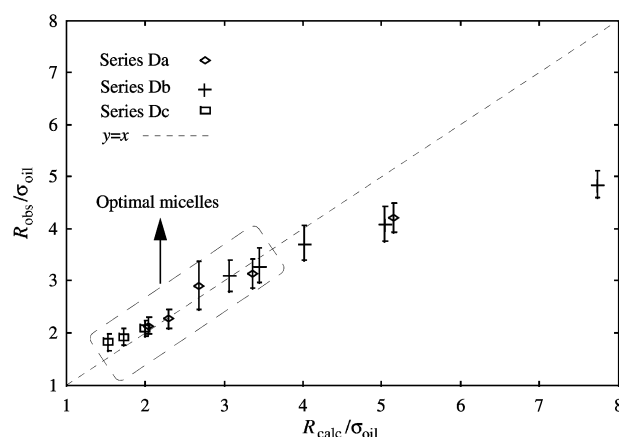


Fig. 11 Comparison between the calculated (from eqn. (19)) and MD micellar radii for all simulations that formed micelles in simulation series Da, Db and Dc.

surfactant molecules, should result in a greater increase in the surface area the surfactant can cover, A_{surf} , than the surface area presented by the water, A_{water} . Hence, increasing the number of water particles and surfactant molecules while preserving the ratio of all components should result in a micelle with surface that is more effectively, or more optimally, covered by surfactant molecules. Improved agreement between the calculated and observed average micellar radius should then be facilitated by increasing the total number of particles in the system size while preserving the ratio of the components. This will only apply to the simulations where one micelle is observed and particularly to the systems where the interface is only sparsely populated by surfactants (*e.g.*, Db1).

To test the idea that the system size is having an effect on the results of the cluster size analysis, two further simulations were performed with the same ratio of water to surfactant as for simulations series Db and Dc, but with more molecules of each type, on a *pro rata* basis. Details of these additional simulations, Db1 and Dc1, are given in Table 7. Fig. 12 shows the results of large water-rich simulation series Db1 and Dc1. Comparing this figure to Fig. 11, the agreement with the theory shows some improvement. The fit between observed and calculated micellar radii shows an improvement for simulations Db13 and Db14. Simulation Db15 shows the same (good) fit between the observed and theoretical cluster radius as simulation Db5. The observed radii from simulations Db11 and Db12, although still smaller than expected, are slightly larger than the corresponding simulations Db1 and Db2. This suggests that the increased system size has improved the correlation between observed and calculated values of the micelle size. However, this increase in the number of components in the system is clearly not enough even for simulations Db11 and Db12, in which the surfactants have an infinite radius of curvature after all. The results of the larger surfactant-rich simulation series Dc1 are in much-improved agreement with the calculated average micelle radius. Noticeably, simulation Dc12 showed well-defined discrete water swollen reverse micelles, whereas at the lower system size (Dc2) the system self-assembled into non-spherical pockets of water interconnected by surfactants. For lower surfactant radii of curvature, there is improved agreement between the simulation and calculated values. This may be due to an increased number of micelles when compared with simulation series Dc that yield a more accurate average cluster radii. Fig. 12 gives a comparison of the simulation and calculated micellar radii for all simulations that self-assembled into discrete micelles. This highlights the improved match for simulations that were repeated at greater system size (Db and Db1, Dc and Dc1) and clearly shows a good correlation between the calculated and observed values for the lower radius of curvature systems (*i.e.*, smaller micelles). Deviations from the expected values are most apparent where only one micelle had formed, the reason for which may be an insufficient number of water and surfactant molecules to form an optimally stable micelle.

Conclusions

We have carried out 'mesoscale' molecular dynamics, MD, simulations of model oil, water and surfactant systems at

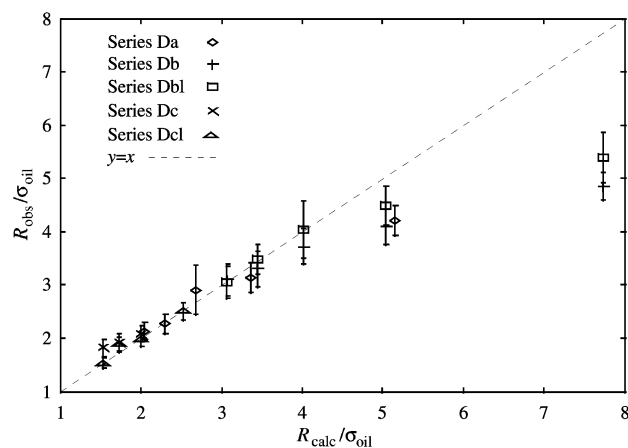


Fig. 12 Comparison between the calculated (from eqn. (19)) and observed micellar radii for all simulations that formed micelles in simulation series Da, Db, Dc, Db1 and Dc1.

selected points in the ternary phase diagram. The surfactant molecule was represented by a Hooke's law dumbbell, the 'water' component with equal or smaller diameter than the 'oil' moiety. The oil and water molecules were represented by spheres of various relative diameters. The model systems self-assembled into the phases expected from the phase diagram, including a bicontinuous phase for the infinite radius of curvature surfactants ($\kappa = 1$) and micelle formation for the oil rich systems. The bicontinuous phase could be broken up into micelles using the smaller radius of curvature surfactants.

Oil-rich simulations were carried out, which showed self-assembly of water and surfactant molecules into micelle-like structures. With decreasing radius of curvature of the surfactant molecule, the micelles broke up into smaller micelles. This tended to be a somewhat discontinuous process for surfactant-poor systems, though, and the micelles were larger in this case also. The number of molecules present in the simulations needed to be enough to form micelles of an optimal size for the selected ratio and geometries of the components. For example, the oil-rich water-swollen systems had a tendency to form 'tube' or rod-like micelles (taking advantage of the periodic boundary conditions as an additional stabilising mechanism) as a substitute for end-capping. The larger water content system (by *ca.* 40%) resulted in a single micelle. A decrease in the radius of curvature of the surfactant molecule generally resulted in an increase in the number of isolated particles and the number of clusters, with a decrease in the maximum and average number of water-like particles in them.

The average size and shape of the micelles were also determined. This analysis showed that micelles are only roughly spherical over a time interval in excess of $t = 25$ reduced units, and that systems with multiple micelles had on average more spherical micelles on this time scale. Over the longer time, $t = 1000$, the average shape of all the micelles was very close to spherical. An asphericity order parameter was also calculated, which showed that the shape of the micelle fluctuated quite dramatically over a short time interval of *ca.* $\Delta t = 10$ –20. However, the average shape of the micelle was spherical, indicated also by values of A_3 close to zero.

Comparison of the average radii of the micelles in a simulation with a popular formula proved to be inaccurate because the surfactant headgroup is assumed to contribute no volume to the core of the water-swollen micelle in this treatment. A modified approach that corrected this was derived and shown to give a much-improved correlation between the simulation and revised theory. Nevertheless, noticeable discrepancies between the revised theoretical model and the

Table 7 Details of increased system size simulations

Simulation index	$N_o : N_w : N_s$	N_o	N_w	N_s	% surfactant
Db1	20 : 2 : 1	3296	352	176	4.60
Dc1	20 : 1 : 2	3120	176	352	9.62

simulation results were still present for model systems that produced a single micelle with large radii of curvature surfactants. This suggests a guiding rule of thumb in simulations of this kind, that micelles with an optimum size can only be presumed when more than one micelle forms in the system. There are still differences between the predicted and observed micelle radius, even with this modified theory, because of the limited number of particles present in a simulations. For example, using eqn. (19) to calculate the radius of the micellar core, for simulation Db1 we have a value of $7.7 \sigma_{\text{oil}}$. At a ratio of number of oil to water to surfactant molecules of 20 : 2 : 1, this would require a system comprising of at least 15500 oil particles, 1550 water particles and 775 surfactant molecules to form a single micelle in an optimum state. Furthermore, to ensure that the micelles present in the simulation are of an optimum size, we would ideally prefer to have enough particles to form at least two micelles of equal size. This would result in a simulation involving at least 35650 particles, which represents a computational burden well beyond the current computing capability, at least on a routine basis.

Acknowledgements

CAB thanks Adibis Ltd for the provision of a research studentship.

References

- 1 J. Israelachvili, *Colloids Surf. A*, 1994, **91**, 1.
- 2 H. T. Davis, *Colloids Surf. A*, 1994, **91**, 9.

- 3 J. N. Israelachvili, *Intermolecular and Surface Forces*, Academic Press, London and New York, 2nd edn., 1991.
- 4 D. J. Mitchell and B. N. Ninham, *J. Chem. Soc., Faraday Trans. 2*, 1981, **77**, 601.
- 5 J. C. Wheeler and B. Widom, *J. Am. Chem. Soc.*, 1967, **90**, 3064.
- 6 B. Widom, *J. Phys. Chem.*, 1984, **88**, 6508.
- 7 M. Schick and W.-H. Shih, *Phys. Rev. B*, 1986, **34**, 1797.
- 8 M. Schick and W.-H. Shih, *Phys. Rev. Lett.*, 1987, **59**, 1205.
- 9 J. W. Halley and A. J. Kolan, *J. Chem. Phys.*, 1988, **88**, 3313.
- 10 G. Gompper and M. Schick, *Phys. Rev. Lett.*, 1989, **62**, 1647.
- 11 B. M. Boghosian, P. V. Coveney and A. N. Emerton, *Proc. R. Soc. London, Ser. A*, 1996, **452**, 1221.
- 12 A. N. Emerton, P. V. Coveney and B. M. Boghosian, *Phys. Rev. E*, 1997, **55**, 4137.
- 13 M. M. Telo da Gama and K. E. Gubbins, *Mol. Phys.*, 1986, **59**, 227.
- 14 B. Smit, P. A. J. Hilbers, K. Esselink, L. A. M. Rupert, N. M. van Os and A. G. Schlijper, *J. Phys. Chem.*, 1991, **95**, 6361.
- 15 K. Esselink, P. A. J. Hilbers, N. M. van Os, B. Smit and S. Karaborni, *Colloids Surf. A*, 1994, **91**, 155.
- 16 S. Karaborni, K. Esselink, P. A. J. Hilbers and B. Smit, *J. Phys.: Condens. Matter*, 1994, **6**, A351.
- 17 K. J. Klopfer and T. K. Vanderlick, *Colloids Surf. A*, 1995, **96**, 171.
- 18 B. Smit, K. Esselink, P. A. J. Hilbers, N. M. van Os, L. A. M. Rupert and I. Szeifer, *Langmuir*, 1993, **9**, 9.
- 19 S. Karaborni, N. M. van Os, K. Esselink and P. A. J. Hilbers, *Langmuir*, 1993, **9**, 1175.
- 20 M. Laradji, O. G. Mouritsen, S. Tøxvaerd and M. J. Zuckermann, *Phys. Rev. E*, 1994, **50**, 1243.
- 21 B. H. Robinson, *Chem. Br.*, April, 342, 1990.
- 22 J. Rudnick and G. Gaspari, *Science*, 1987, **237**, 384.
- 23 G. D. Rees and B. H. Robinson, *Adv. Mater.*, 1993, **9**, 608.
- 24 J. N. Israelachvili, D. J. Mitchell and B. W. Ninham, *J. Chem. Soc., Faraday Trans.*, 1976, **72**, 1525.
- 25 S. Jashy, M. Al-Naghy and M. de Llano, *Phys. Rev.*, 1987, **35**, 1376.
- 26 A. Santos, M. Lopez de Haro and S. Bravo Yuste, *J. Chem. Phys.*, 1996, **103**, 4622.